Appl. Phys. B 86, 197–208 (2007)
DOI: 10.1007/s00340-006-2528-z

Applied Physics B
Lasers and Optics

Invited paper

J.A. L'HUILLIER[1,✉]
G. TOROSYAN[2]
M. THEUER[2]
C. RAU[1]
Y. AVETISYAN[3]
R. BEIGANG[1,2]

Generation of THz radiation using bulk, periodically and aperiodically poled lithium niobate – Part 2: Experiments

[1] Technical University of Kaiserslautern, Department of Physics, Erwin-Schroedinger-Strasse 46, 67663 Kaiserslautern, Germany
[2] Fraunhofer IPM, Terahertz Measurement and Systems, Erwin-Schroedinger-Strasse 46, 67663 Kaiserslautern, Germany
[3] Microwave Engineering Department, Yerevan State University, 1 Alek Manoogian Street, Yerevan 375049, Armenia

Received: 11 August 2006
Published online: 13 December 2006 •

ABSTRACT Optical rectification of femtosecond pulses in nonlinear materials is an efficient method to generate ultra-short terahertz (THz) pulses in a wide frequency range extending from 100 GHz to well above 10 THz. Lithium niobate (LN) is well suited for such a purpose despite the high absorption in the THz range. In this part we will focus on the various experimental realizations to produce THz radiation in bulk, periodically, aperiodically and two-dimensionally poled LN. The possible bandwidth, tunability and the techniques to overcome the high absorption will be discussed as well.

PACS 42.65.Ky; 42.70.Mp; 42.72.Ai

1 Introduction

The generation and application of THz radiation using photonic techniques has attracted considerable interest over the past years. Among the different optical techniques of THz generation the optical rectification (OR) of a fs-laser pulse in a nonlinear crystal, i.e. difference-frequency generation (DFG) between frequencies within the broad spectrum of the same pulse, has turned out to be extraordinarily well suited. In Part 1 [1] of this review the possibility of THz emission was theoretically considered taking into account a direction different from the fs-pulse propagation. From this discussion it is clear that the main difference in the various schemes of OR to generate THz radiation is the way to achieve phase-matched THz generation and to reduce the THz-wave decay in the nonlinear crystal. While the first part focused on the theoretical description, the following discussion will focus on the experimental realizations of the theoretical concepts discussed in Part 1. Similar to the outline of Part 1 we will discuss the various methods in bulk materials and proceed afterwards with one-dimensional quasi-phase matched (QPM) structures (ppLN, AppLN) and two-dimensional QPM structures (TppLN).

Beginning with ferroelectric materials like lithium niobate (LN) [2–8] or lithium tantalate [9] via semiconductor materials like GaAs [10, 11], GaSe [12, 13] or $ZnGeP_2$ [14] to organic materials like the organic salt DAST (4-dimethylamino-N-methyl-4-stilbazolium-tosylate) [15, 16] or polymers [17, 18], a wide range of different materials have been used for THz generation by OR of fs-laser pulses. All of these materials have particular advantages and inherent difficulties. As a nonlinear material LN has turned out to be extraordinarily well suited for this purpose. This is because of its high nonlinearity [19, 20], high transparency in the visible and near-infrared spectral region [21] and the well-developed poling technique [20, 22, 23] for this material. The major drawback of this material is the high absorption at THz frequencies [24, 25]. The intensity absorption coefficient α increases from around 12 cm^{-1} at 1 THz to more than 170 cm^{-1} at 2.5 THz [25, 26].

The main origin of this strong absorption is the low-frequency tail of the transverse optical phonon mode at 7.6 THz [25, 27]. Recently published detailed measurements performed by Palfalvi et al. [24] show that the absorption depends on the stoichiometry and on the MgO doping concentration, which is often used to reduce the photorefractivity of LN. The absorption decreases in 0.7% Mg doped stoichiometric LN (sLN) to 82.6 cm^{-1} at 2.4 THz, which is still considerably higher than the absorption in the visible (VIS) or near infrared (NIR). A significant reduction of the absorption can be achieved by cooling to cryogenic temperatures [24]. This method was utilized to enhance the THz wave output [28], but is hardly practicable for many applications. Therefore, concepts to minimize the path length inside the crystal are still of high interest. Due to the high dielectric contribution of the transverse optical phonon mode to the refractive index, the value of the refractive index in the THz range is more than twice as high as the refractive index in the NIR or VIS. Therefore, it is difficult to use the natural birefringence to obtain phase matching in LN for efficient THz generation.

Despite these problems the material properties of LN are still a reasonable compromise for the requirements for a THz source based on frequency conversion of NIR radiation. The remaining constraints have been partly overcome by various concepts to reduce in particular the high absorption of LN. This is one reason why this material is still widely used for THz generation. Therefore, we focus the exemplary discussion on LN.

✉ Fax: +49-631-205-3906, E-mail: huillier@physik.uni-kl.de

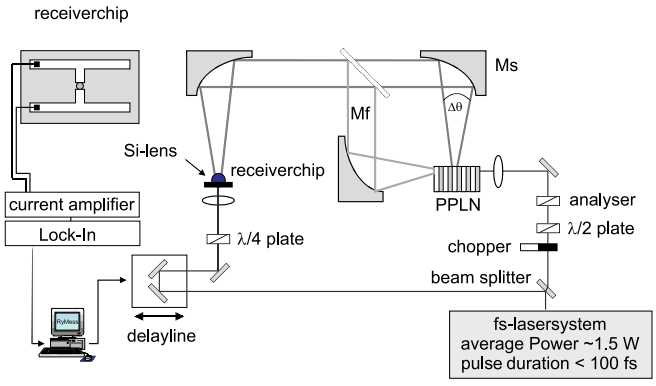

FIGURE 1 Experimental setup for the generation and detection of THz radiation. With this setup the radiation in the forward direction as well as the radiation in the sideways direction (surface emission or Cherenkov-like radiation) can be investigated

2 Experimental setup

The typical experimental setup used in the experiments is shown in Fig. 1. The setup consists of a Ti:sapphire laser (Spectra Physics, Tsunami), which provides sub-100-fs pulses with a repetition rate of 80 MHz and an average power of ~ 1.5 W. The collimated laser beam is split into two beams. One beam is used to trigger the detector behind a delay line and the other beam is focused into the sample. The crystal is positioned within the Rayleigh length of the focus of the NIR radiation. The emitted THz radiation is collected and focused by two spherical silver mirrors onto the detector. The detector was a standard silicon on sapphire (SOS) or low temperature (LT)-GaAs photoconductive antenna with a typical dipole length of 50 μm. Using two sets of mirrors, Mf and Ms, the THz radiation in the forward direction and a direction perpendicular to the surface can be observed, respectively.

Besides the observation direction the various realizations differ in the type or structure of the nonlinear medium LN. A detailed discussion of the particular structures will be given in the corresponding sections.

3 Bulk lithium niobate (LN)

3.1 *Optical rectification*

As early as 1962 optical rectification in electro-optic media was reported [29]. Optical rectification of fs pulses is in fact collinear difference frequency generation between particular spectral components within the ultra-short laser pulse [30]. In 1992 Xu et al. [31] investigated the generation of THz radiation in electro-optic materials (here LN and $LiTaO_3$) due to the interaction with fs optical pulses. Two years later Carrig et al. compared the efficiency of LN, $LiTaO_3$ and DAST [32] and reported the power scaling of THz radiation. These results showed that despite the low damage threshold of DAST the performance is superior to LN and $LiTaO_3$. Further experimental realizations of this scheme have been demonstrated in many experiments. But, in this case of non-phase-matched DFG the THz radiation is emitted only from entrance and exit surfaces of the crystal within the coherence length defined by

$$l_c = \frac{\pi}{\omega_{THz}} \frac{c}{|n_g - n_{THz}|} . \quad (1)$$

With typical values for both refractive indices in LN ($n_g = 2.3$ and $n_{THz} = 5.17$ [25]) the coherence length is ~ 50 μm and therefore only a small part near both surfaces of the crystal is used. A sketch of a typical crystal and the coordinate system is shown in Fig. 2.

For the comparison with the other methods discussed in this paper, we used a 1-mm-thick x-cut LN crystal to produce THz radiation. Figure 3a shows the electric field of the generated pulses. As expected, the electric field in the time domain consists of two cycles. The delay between the two peaks is $\Delta t = 9.5$ ps. Due to the simple relationship between the length of the crystal and the delay time [1, 31],

$$\Delta L = \frac{c}{\Delta n} \Delta t , \quad (2)$$

this results in $\Delta L = 1$ mm, which is in good agreement with the sample length L. The amplitude of the second peak (larger delay) is smaller than the amplitude of the first peak (shorter delay). This behavior can easily be understood if we take the absorption and the refractive index of LN in the THz range into account. Since the refractive index of LN is around 5.1 in the THz range, the second cycle corresponds to the radiation generated at the entrance facet of the sample (see also the theoretical discussion in Part 1 [1]). The radiation forming the second peak took a path length of ≈ 1 mm in LN while the first peak is generated very close to the exit surface. Therefore, higher absorption losses occur for the second peak, resulting in a lower amplitude.

The Fourier transform gives the spectrum shown in Fig. 3b. The obtained spectrum covers a frequency range of ≈ 1.6 THz. The envelope is related to the pulse duration of the Fourier-limited fs pulse (see Part 1 [1]). The measured bandwidth is limited mainly by the bandwidth of the fs pulses and the bandwidth of the detector. In addition, the absorption strongly increases for higher frequencies, resulting in a further limitation of the bandwidth. This behavior will be discussed in detail in Sect. 3.2.

Opposite to the envelope, the oscillations result from destructive interference of particular frequency components. The destructive interference occurs for components whose coherence lengths fit $2 \times n$ times into the crystal length (with an integer n).

Despite the high absorption of LN for THz frequencies [24, 25] in this scheme only small absorption losses for the first THz pulse (first peak in Fig. 3a) occur, due to the gen-

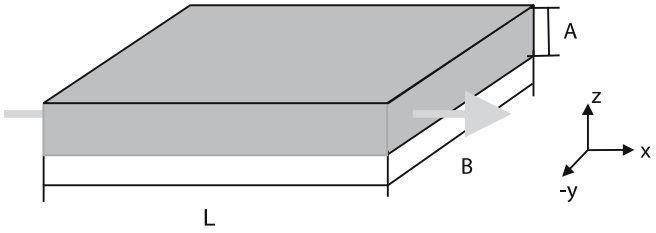

FIGURE 2 Scheme of the sample and coordinate system used for the THz generation in bulk LN

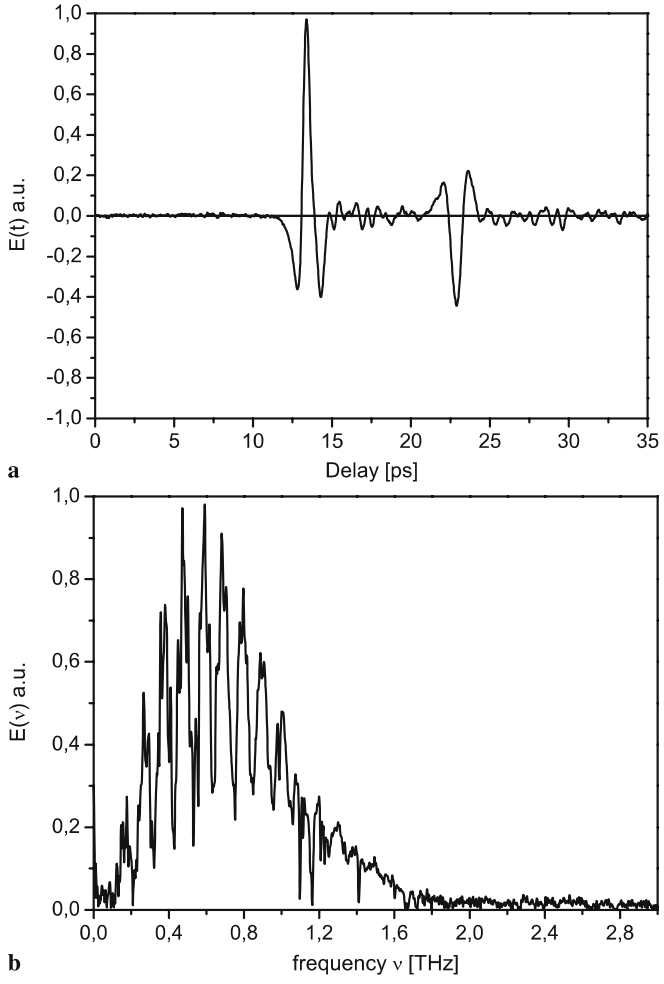

FIGURE 3 Optical rectification (non-phase-matched DFG): (**a**) electric field, (**b**) frequency spectrum

eration very close to the exit surface. But, the generated power for DFG scales with the square of the interaction length up to the coherence length. Due to the short coherence length the generated power for non-phase-matched DFG is strongly limited.

3.2 *Cherenkov radiation*

To improve the THz generation output it is necessary to obtain phase matching between the participating waves. One way is to use Cherenkov radiation. The analogue of the Cherenkov radiation from superluminal charged particles for intense light pulses was predicted by Askaryan in 1962 [33]. More than 20 years later the effect was demonstrated experimentally [34, 35] for microwave and THz-wave generation by pumping with ultra-short optical pulses.

When the wave packet of an ultra-short optical pulse propagates through a bulk of electro-optical material, the generated Cherenkov radiation composes a cone around the direction of propagation. In this case under a single defined angle to the direction of the NIR beam the particular THz waves generated at different points in the crystal are in phase. This angle is called the Cherenkov angle Θ_C and it is given by (see also Part 1 [1])

$$\Theta_C = \arccos\left(\frac{n_g}{n_{THz}}\right) . \quad (3)$$

For typical values of the group index of LN in the NIR of $n_g = 2.3$ and the refractive index at a frequency of 1 THz of $n_{THz} = 5.17$ the angle is $\Theta_C = 63.6°$.

As a consequence the THz radiation hits the surface of a conventional rectangular shaped LN crystal under an angle of $\approx 26°$ to the normal. Due to the very high refractive index of LN in the THz range the angle of total reflection is only around 11°. The THz radiation is therefore totally reflected and absorbed inside the LN crystal. To allow the THz radiation to exit the crystal–air interface in the normal direction without refraction, one has to take special care. Hu et al. [36] used a setup where the exciting laser beam has an incident angle of $< 27.4°$. The refraction of the beam at the crystal–air boundary results in a propagation direction not parallel to the crystal's boundary. By changing the incident angle the angle between the emitted Cherenkov radiation and the exit surfaces can be adjusted suitably. But, in this setup only a limited length can be used.

To avoid this problem typically a plate with wedged exit surfaces is used. In the case of LN the wedge angle is about 26°. So, the THz radiation can pass the surface. This is schematically shown in Fig. 4a. However, the path length of the generated radiation inside the crystal and therewith the absorption losses increases, since the radiation is not produced close to the surface.

For a further improvement of the output coupling efficiency and spectral bandwidth, the wedged part of the crystal can be replaced by a silicon prism [6]. A schematic of this geometry is shown in Fig. 4b. This setup was originally developed by Kawase et al. [37] for the extraction of THz radiation from a ns-pumped THz optical parametric oscillator in a non-collinear setup. The absorption for the THz radiation in silicon is much lower and the refractive index ($n \sim 3.4$ [38]) is in between the refractive indices of air and LN. So, the THz radiation can pass the surfaces without total internal reflection and less Fresnel losses. If the NIR beam is placed near the interface between the LN crystal and the silicon prism, the absorption in LN is minimized.

For the experimental comparison of both schemes again the setup shown in Fig. 1 is used. The sample was replaced by a wedged crystal, the sideways detection was used and the detection geometry was adjusted accordingly.

The experimentally obtained electric field amplitude and spectrum for the first scheme, shown in Fig. 4a, are plotted in Fig. 5 a and b, respectively.

The electric field amplitude consists, as expected, of a single cycle and the spectrum covers more than 4 THz limited by the spectral bandwidth of both the pump pulse and the detector. The spectrum shows various absorption lines of water. During the experiments no special care was taken to remove the water vapor from the air, because these absorption lines do not disturb the aimed comparison of the different generation schemes.

In Fig. 6a and b the experimentally obtained spectra for a wedged MgO:LN crystal (solid line) and a MgO:LN sample with a silicon prism as an output coupler (dotted line) are shown for two different focal lengths [6].

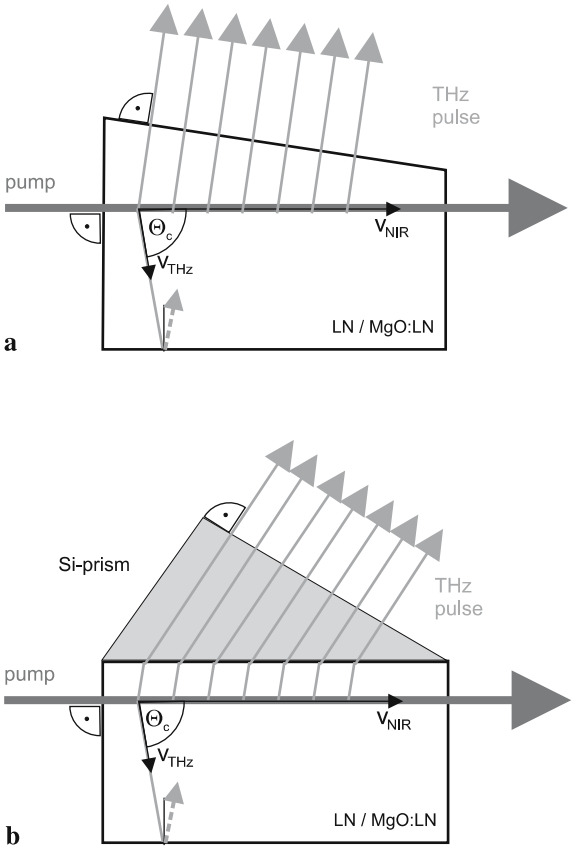

FIGURE 4 Schematic diagram of the crystal shape for the extraction of Cherenkov-type THz radiation: (**a**) crystal with a wedged surface, (**b**) crystal with a silicon prism

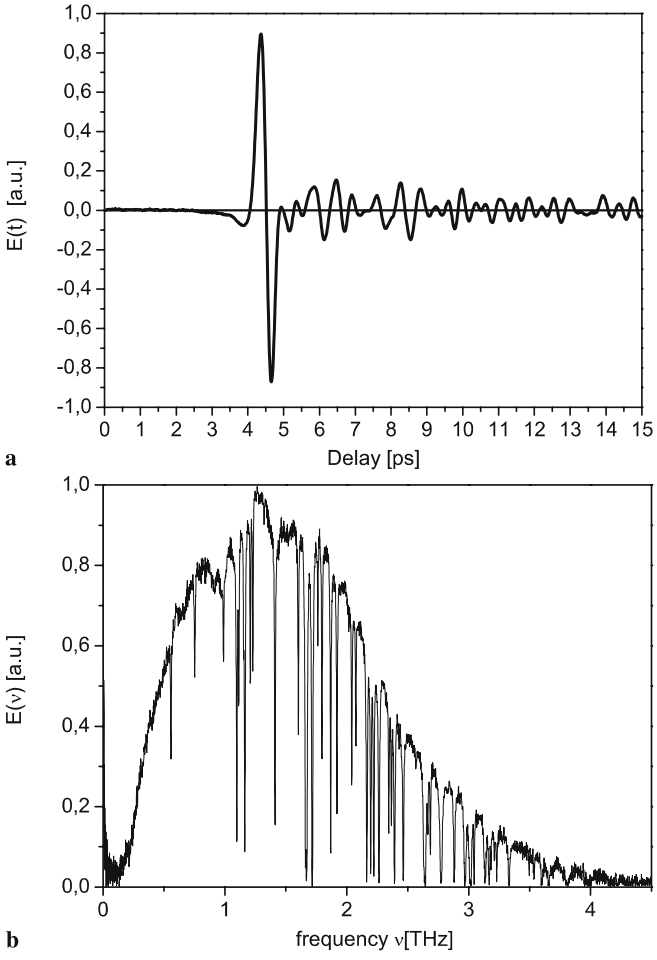

FIGURE 5 Cherenkov radiation: (**a**) single-cycle electric field, (**b**) frequency spectrum for a wedged LN sample

From a comparison of the different focal lengths it is obvious that a shorter focal length results in a broader spectrum. This is the expected result from the theoretical discussion [1]. In addition, it is seen that the obtained bandwidth of the THz radiation with the wedged sample is smaller compared to the setup with the Si prism. This behavior can be easily understood if we take into account the strong and frequency-dependent absorption. The absorption strongly increases for higher THz frequencies [25]. This results in a smaller amplitude for higher THz frequencies compared to the obtained amplitude for lower THz frequencies.

The frequency-dependent absorption can be included in the theoretical description (see (21) in Part 1 [1]) by adding an exponential factor (Beer's absorption law). For simplicity, we assume a constant path length s inside LN for the THz radiation generated at different points of the crystal. This is at least valid for the setup with the silicon prism. With this assumption, we obtain

$$E_\Theta(\omega, R, \Theta_x) \sim G'(\omega, \Theta_x) F(\omega, \Theta_x) \mathrm{e}^{-\frac{\alpha(\omega)}{2} s}\,, \tag{4}$$

with the relations $G'(\omega, \Theta_x) = G(\omega, \Theta_x) H(\omega, r_0)$ and $F(\omega, \Theta_x) = \mathrm{sinc}\,(\omega L \Delta n / 2c)$ given in Part 1 [1]. $\alpha(\omega)$ denotes the intensity absorption coefficient.

With the empirical relation and experimental data for the frequency-dependent absorption $\alpha(\omega)$ obtained by Schall et al. [25] an analytical calculation is possible. Figure 7 shows the calculated spectra for different path lengths inside LN. The calculation was performed with (4) and the pulse duration ($\tau = 100$ fs) and the beam waist ($\omega_0 = 30$ μm) used in the experiments.

From Fig. 7 it is clear that with an increasing path length inside LN the amplitude and the bandwidth decrease and the maximum of the electric field moves towards lower frequencies. This is the expected behavior caused by the increasing absorption at higher THz frequencies. A further problem arises from the fact that the beam width of the NIR beam should be in the order of the THz wavelength to obtain constructive interference between the partial waves generated at different points. To obtain a reasonable bandwidth and power it is necessary to obtain a small focus in the medium. Therefore, the power scaling in this scheme is limited due to radiation damage.

4 Periodically poled lithium niobate (ppLN)

Phase matching for optical nonlinear processes in the visible and NIR spectral range is normally obtained by birefringence phase matching [39], by quasi-phase matching in periodically poled ferroelectrics [40] or a combination of both [41].

In fact, the natural birefringence of GaSe has been used to obtain phase matching for the generation of far-infrared (FIR)

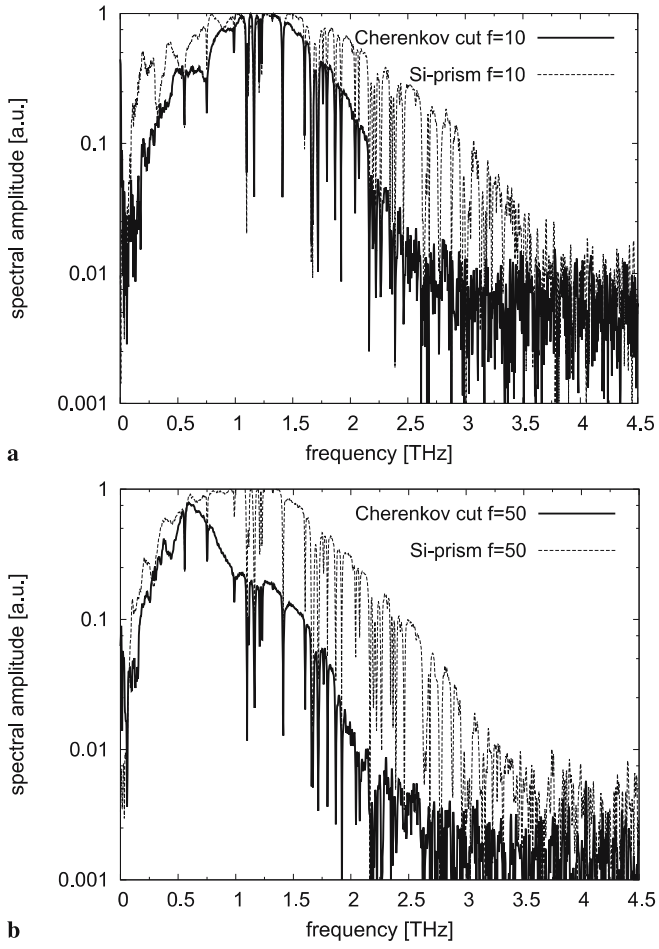

FIGURE 6 Measured Cherenkov-type THz spectra for wedged MgO:LN (*solid line*) and a Si-prism output coupling (*dotted line*) for different focal lengths (**a**) $f = 10$ mm and (**b**) $f = 50$ mm

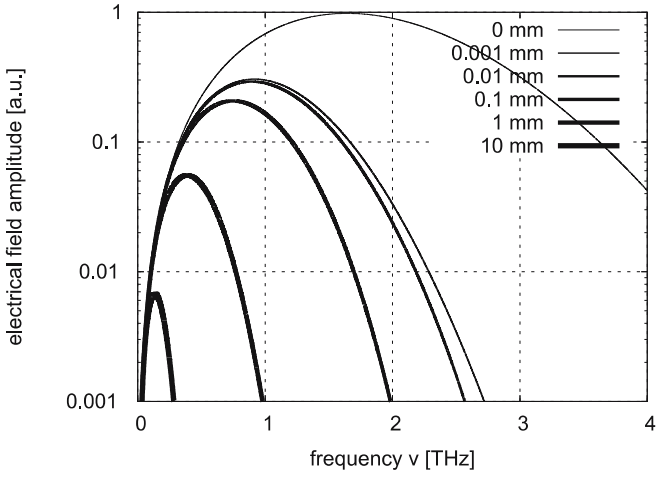

FIGURE 7 Calculated spectra for different path lengths inside LN, a pulse duration of $\tau = 100$ fs, a beam waist of $\omega_0 = 30\,\mu$m and the absorption coefficient obtained by Schall et al. [25]

radiation [42]. But, phase matching using the natural birefringence is difficult or even impossible below but close to the phonon frequency [43].

While birefringence phase matching is not preferable, quasi-phase matching is still a versatile possibility [4, 7, 44–48]. In contrast to optical rectification and Cherenkov radiation obtained from bulk LN, THz generation in ppLN leads to tunable narrowband THz radiation.

A sketch of a periodically poled crystal is shown in Fig. 8. The necessary poling periods vary between 10 microns (10 THz) and 400 microns (300 GHz). In the theoretical discussion [1] an analytical relation between the poling period Λ and the center frequency $\nu = \omega/2\pi$ of the THz radiation was obtained (see (28) in Part 1), which can be written in the form

$$\Lambda = \frac{1}{\nu} \frac{c}{\left| n_{\mathrm{g}} - n_{\mathrm{THz}}(\nu) \cos \Theta \right|} . \tag{5}$$

The angle Θ describes the direction of observation. Angles $\Theta = 0$ and $\Theta = \pi$ correspond to emission in forward and backward directions, respectively.

Please note that the refractive index in the THz range varies between 5.17 at 1 THz and 5.8 at 3 THz [25] while the variation of the refractive index between the particular components of the NIR fs pulse is very small.

4.1 *Forward and backward emission*

The generation of narrowband THz radiation by quasi-phase-matched OR in ppLN was first reported by Lee et al. [44, 45].

They found in addition to the THz emission in the forward direction ($\Theta = 0$) an additional emission in the backward direction ($\Theta = \pi$). For a typical poling period of $\Lambda = 120\,\mu$m the calculation results in THz frequencies of 0.87 THz and 0.34 THz for forward and backward directions, respectively.

QPM structures allow a definition of both the center frequency (see (5)) and the bandwidth. For the experimental realization the setup for the forward direction is used (mirrors Mf, see Fig. 1). The setup is very similar to the setup for optical rectification in bulk LN (see Sect. 3.1). Only the bulk LN crystal has been replaced by a ppLN sample. The typical crystals used for our investigations had a poling period of $\Lambda = 120\,\mu$m. The samples were 0.5-mm thick and had a length of 10 mm. Figure 9a and b show the experimentally and numerically obtained electric field in the time domain observed in the forward direction.

From Fig. 9 it is clear that the amplitude of the electric field decreases exponentially with an increasing delay. This behavior can easily be understood if again the different velocities and absorption for the NIR and the THz radiation are considered. The NIR radiation is much faster than the THz radiation. Therefore, the radiation generated in the poling

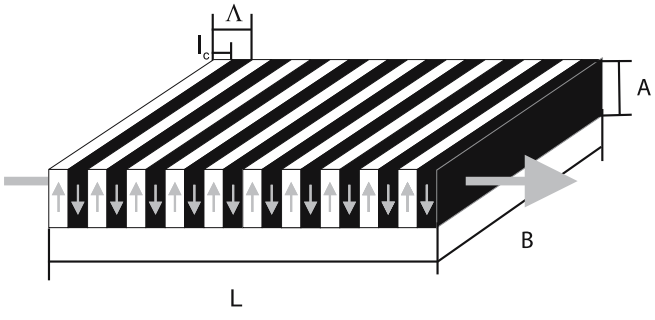

FIGURE 8 Scheme of the samples typically used for the THz generation in periodically poled LN (ppLN)

period at the exit surface of the ppLN crystal arrives first at the detector. In addition, due to the shortest path length inside the crystal, the lowest absorption occurs and therefore the largest electric field amplitude is obtained. With an increasing path length inside the ppLN crystal the delay and the absorption increase. Similar to the discussion in Sect. 3.2, the high absorption can be included in a quantitative approach by considering an exponential factor (Beer's absorption law) in the theoretical description. This additional factor results in the observed decay of the field amplitude for longer path lengths inside the crystal.

The number of cycles of the electric field corresponds to the number of periods which contribute to the electric field [1]. Therefore, from the 40 visible cycles in Fig. 9 a a usable crystal length of 4.8 mm can be calculated. This means that the usable length for the THz generation is strongly limited by the high absorption of LN, while the usable length for applications of ppLN in the VIS or NIR spectral range is limited mainly by the poled crystal length.

For a comparison of the experimentally obtained electric field and the theoretical prediction, the numerically calculated electric field is shown in Fig. 10b. To compare the numerical and experimental results the graph from Fig. 9a is filtered to suppress the oscillations caused by the emission in the backward direction and is also plotted in Fig. 9b. To obtain a reasonable agreement between theory and experiment a poling period of $\lambda = 120.7\,\mu\text{m}$ and an absorption which is a factor of 1.4 higher than in the measurements of Schall et al. [25] were used for the calculation. The first correction can be explained by a slightly rotated crystal and the second correction may attributed to the crystal and its composition in this particular case.

Figure 10a and b show the spectrum calculated by a Fourier transformation of the electric field. From Fig. 10b it is obvious that the theoretical and experimental results fit very well. The theoretical center frequency ν calculated by (5) using the parameters $\Lambda = 120.7\,\mu\text{m}$, $\Theta = 0$, $n_g = 2.3$ and $n_{THz} = 5.17$ is $\nu = 0.866\,\text{THz}$. This is in good agreement with the experimental result. Besides the main peak in Fig. 10a a second peak at 0.32 THz is observed. This frequency is close to the expected frequency of THz radiation generated in backward emission. Therefore, this radiation can be attributed to THz radiation generated in the backward direction. But, please note that the radiation emitted in the backward direction is detected in the forward direction. This can be explained by two possible schemes. In the first scheme (A) the THz radiation generated in the backward direction is partially reflected at the entrance surface of the LN crystal. Opposite to scheme (A), in scheme (B) the NIR radiation is partially reflected at the exit surface of the crystal. The NIR radiation propagating from the exit surface backward to the entrance surface generates THz radiation similar to the THz radiation in the backward direction in scheme (A). This radiation is the observed radiation in the forward direction.

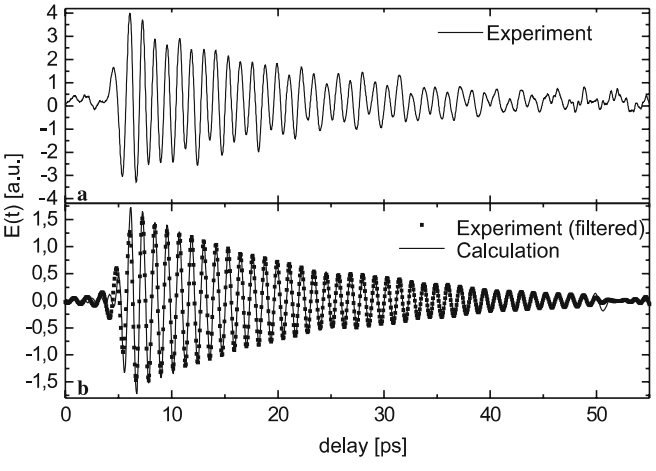

FIGURE 9 (**a**) Experimentally and (**b**) theoretically obtained electric fields of the THz radiation generated in the forward direction in a ppLN crystal with a poling period of 120 μm

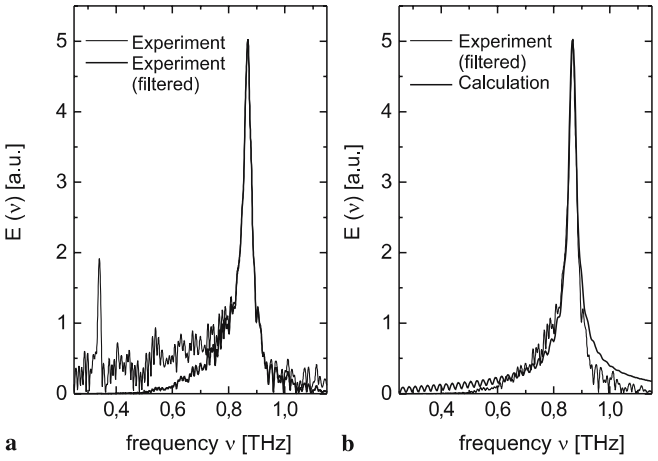

FIGURE 10 (**a**) Experimentally and (**b**) theoretically obtained spectra of the THz radiation generated in the forward direction in a ppLN crystal with a poling period of 120 μm

4.1.1 Frequency tuning. Frequency tuning of the radiation generated by quasi-phase-matched nonlinear optical processes can be obtained by changing the poling period or the temperature [46]. Different ppLN crystals of various poling periods for the generation of THz radiation in a wide range of wavelengths have been used. It is known that various discrete poling periods on a single crystal can be fabricated [49]. The selection of the THz frequency in such a multigrating ppLN crystal can be done by moving the crystal perpendicular to the NIR beam. But, this scheme allows only the selection of a few discrete frequencies. Further fine tuning can be done by changing the temperature of the sample [46].

Experimentally obtained and theoretically calculated frequencies for various poling periods for the THz generation in the forward as well as in the backward direction are plotted in Fig. 11. Besides the results for first-order QPM, the results for third-order QPM in the forward direction are also shown. With poling periods between 10 μm and 400 μm the complete THz range between 0.24 THz and 10 THz can be generated.

Besides using different discrete poling periods a further possibility to continuously tune the poling period is to rotate the crystal [7]. In Fig. 12 a schematic diagram of the setup used is shown. The pump beam passes through the center of the round crystal (which is also the axis of rotation) so that

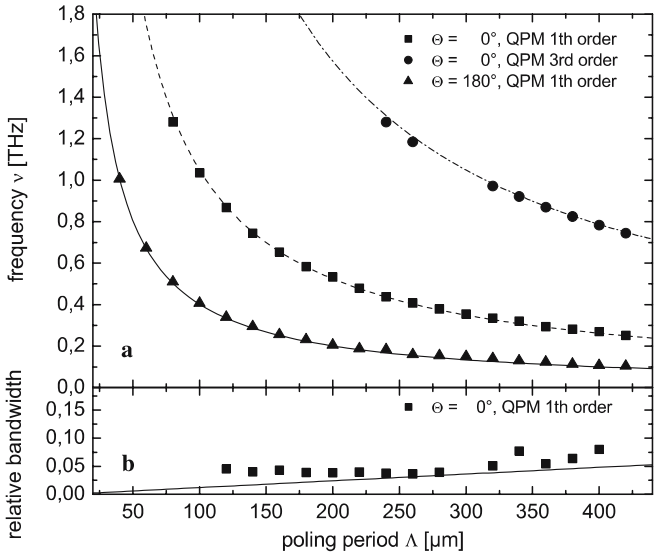

FIGURE 11 Experimentally obtained (**a**) THz frequencies and (**b**) bandwidth depending on the poling period for emission in the forward direction ($\Theta = 0°$) and the backward direction ($\Theta = 180°$)

the beam direction stays constant during the rotation of the crystal. In this way any beam deviation during rotation can be avoided. The effective poling period changes with $1/\cos\alpha$, where α is the angle between the direction of beam propagation and the normal to the poling direction; therefore, the center frequency of the THz radiation generated in the forward direction is given by a modified equation (5):

$$\nu(\alpha) = \nu(0)\cos\alpha = \frac{\cos\alpha}{\Lambda}\frac{c}{\left|n_{\mathrm{g}} - n_{\mathrm{THz}}(\nu)\right|}. \tag{6}$$

With an increasing rotation angle the effective length of the poling period increases, but the number of contributing domains decreases. Equation (6) is valid for small rotation angles as long as a reasonable number of periods contribute to the THz generation.

Due to the decreasing number of contributing domains, the relative bandwidth increases accordingly. The bandwidth can be calculated from the equation obtained for ppLN crystals by considering the rotation angle α:

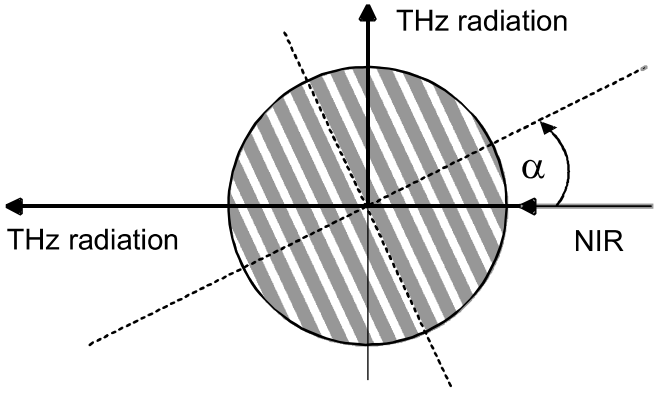

FIGURE 12 Schematic diagram of the circular ppLN crystal used for continuous frequency tuning

$$\frac{\Delta\nu}{\nu} = \frac{1.768}{N}\cos\alpha\,. \tag{7}$$

For the experimental demonstration a round ppLN crystal with a diameter of 7.5 mm and a poling period of 127 μm was used [7]. Figure 13 shows the experimentally obtained tuning curves for the THz frequency (upper graph) and the relative bandwidth (lower graph). The solid line represents the theoretically calculated tuning characteristics and the bandwidth in the upper and lower graphs, respectively. In this experiment a continuous tuning range between 0.18 THz and 0.82 THz with a minimum relative bandwidth of 2.5% has been demonstrated.

4.2 *Surface emission*

One major drawback of the quasi-phase-matched collinear optical rectification discussed above is the inherent long path length inside the crystal. The strong absorption of LN reduces the available output power and limits the number of domains that effectively participate in the THz generation. The last, according to (7), results in a worsening of the monochromaticity of the generated THz wave. A possible solution of this problem is the emission of the generated THz radiation perpendicular to the surface of the ppLN crystal. In this way the path length within the ppLN crystal can be reduced considerably and the area of THz emission can be enlarged, resulting in a smaller divergence and possibly higher output power.

A suitable scheme for surface emission was proposed by Avetisyan and Kocharian [50] and experimentally demonstrated for fs lasers by Weiss et al. [47]. An analytical expression for the expected THz frequency for a given poling period Λ and observation angle Θ has already be given in (5). From that equation it is obvious that a changed observation angle for a fixed poling period results in a changed THz frequency. This can be used to tune the THz radiation by changing the angle of observation. But note that this is very different compared to

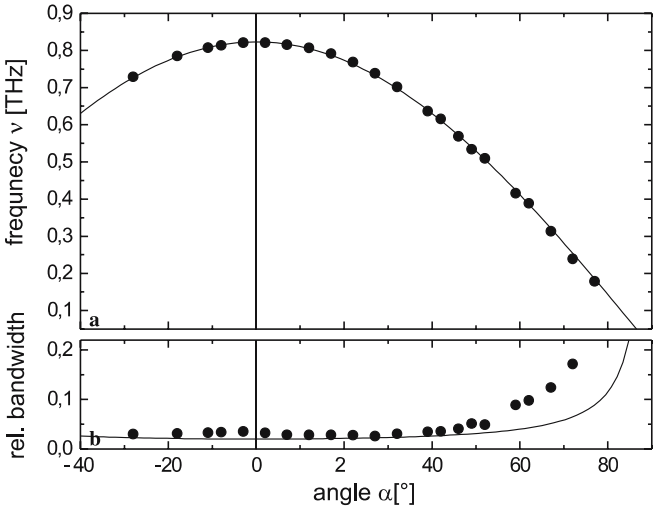

FIGURE 13 (**a**) THz frequency observed in the forward direction as a function of the angle between the direction of propagation and the poling structure. The *solid line* represents the theoretically obtained tuning characteristic; (**b**) relative bandwidth for different propagation angles. The *solid line* represents the calculated relative bandwidth, assuming a rectangular waveform

the method used for the frequency tuning in Sect. 4.1.1. While for the approach in Sect. 4.1.1 the crystal is rotated, for the method discussed in this section the angle of observation is changed. In the first case all participating waves propagate in the forward direction (collinear setup) whereas in the second case only the NIR wave propagates in the forward direction while the THz wave is observed under an angle of Θ (non-collinear setup).

Figure 14 shows the calculated tuning curve for a poling period of $\Lambda = 127\,\mu\text{m}$. The angles $\Theta = 0$ and $\Theta = \pi$ correspond to THz radiation in the forward and backward directions, respectively. These observation directions have been discussed in detail in Sect. 4.1. From Fig. 14 it is clear that for an angle of $\sim 63°$ a singularity exists. This angle is the Cherenkov angle (see (3) discussed in Sect. 3.2). For this angle not a single frequency but broadband THz radiation is emitted.

Similar to the generation of Cherenkov radiation, the possible angle for the extraction of the THz radiation is limited, due to total reflection. The angles for which the generated THz radiation can leave the crystal (besides the forward and backward directions) are marked in Fig. 14 by the gray box. Therefore, we will focus the following discussion on this window.

For the experimental realization the sideways geometry scheme (using mirror set Ms, see Fig. 1) was used. The setup is very similar to the setup for the generation of Cherenkov radiation. Only the crystal was replaced and the focusing as well as the detection angle was adjusted for the detection of sideways radiation under the appropriate angle. For this experiment a 8-mm-long crystal with a poling period of 127 μm was used. Figure 15 a shows the experimentally obtained electric field of the generated pulse.

The Fourier transform results in the spectrum, which is shown in Fig. 15b. The spectrum is centered around 0.94 THz. This result differs from the theoretically expected value of 1.027 THz, which was obtained from (5) for $\Theta = 90°$ and $\Lambda = 127\,\mu\text{m}$. But, for an observation angle of 92.3° the expected center frequency matches the experimentally measured one. A variation of the observation angle of 2.3° is within the experimental accuracy and explains the difference. In the right-hand edge of the spectrum a dip caused by absorption of water vapor is obvious.

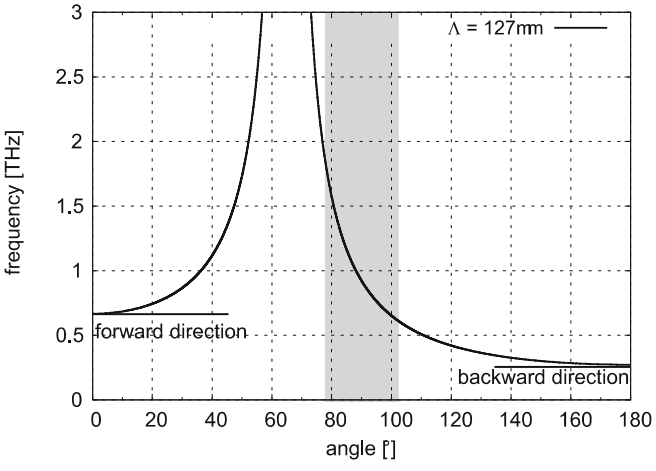

FIGURE 14 Dependency of the difference frequency ν on the angle between the propagation directions of the NIR and THz beams

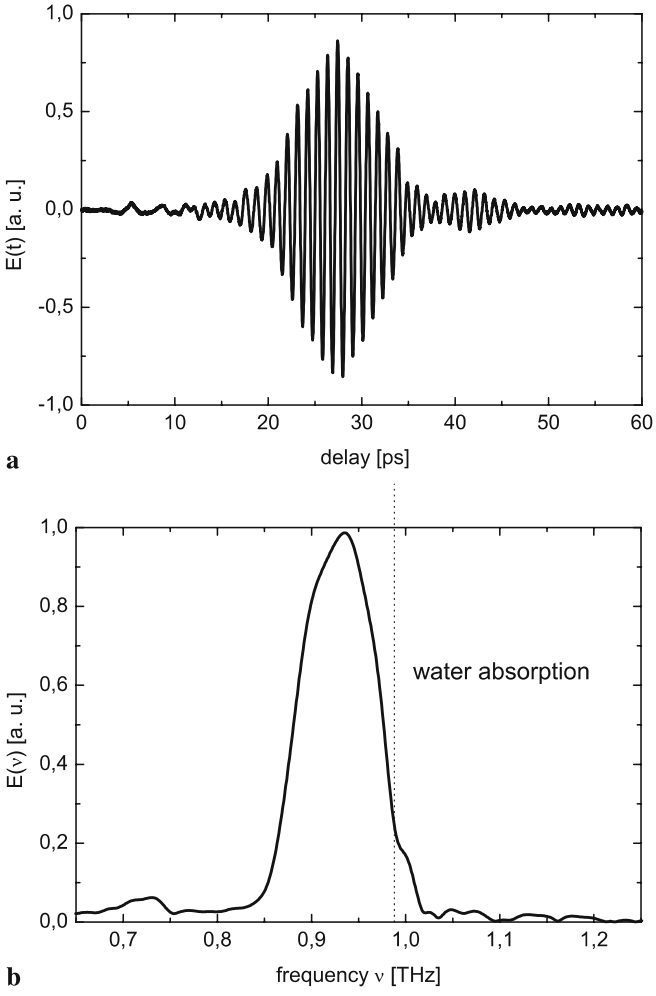

FIGURE 15 Experimentally obtained electric field (**a**) and frequency spectrum (**b**) of the THz radiation generated in surface emission geometry in a ppLN crystal with a poling period of 127 μm

The measured relative bandwidth of the THz radiation is 10% (FWHM). This value is much larger than the theoretically expected value of 2%, which was calculated by (7). The reason for this difference is the sensitivity of the THz frequency to changes in the observation angle and the sensitivity of the detector. This can clearly be seen from Fig. 14. Due to the finite detection angle $\Delta\Theta$ around the observation angle Θ_0 the THz radiation consists of various frequency components around the designed center frequency. An equation for the relative bandwidth can be obtained from (5):

$$\frac{\Delta\nu}{\nu} = \frac{n_{\text{THz}} \sin\Theta_0}{\left| n_{\text{g}} - n_{\text{THz}} \cos\Theta_0 \right|} \Delta\Theta \,. \tag{8}$$

This equation becomes zero for forward and backward radiation and infinite for the Cherenkov angle Θ_{C}, due to the $\sin\Theta_0$ and $\cos\Theta_0$ terms. In the surface emitting scheme the finite detection angle has to be considered. The parabolic mirrors used in the experimental setup have a typical collection angle of $\Delta\Theta = 15°$. With (8) this results in an expected bandwidth of 11%, which is in good agreement with the measurement [47].

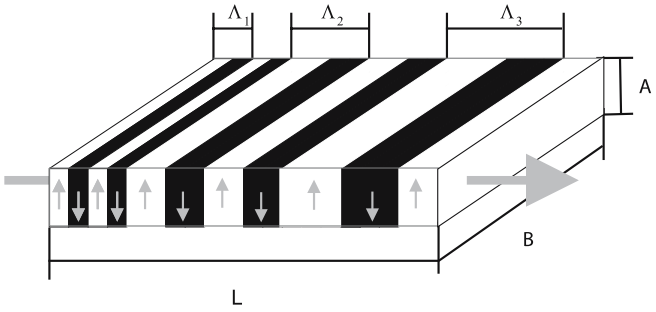

FIGURE 16 Exemplary poling structure for the THz generation in aperiodically poled LN (AppLN)

Therefore, the bandwidth in the sideways emission scheme is mainly limited by the collection angle and can be adjusted suitably for a particular application. A reduction of the bandwidth in the surface emitting scheme can be obtained by using slits behind the ppLN.

5 Aperiodically poled lithium niobate (AppLN)

Up to now we discussed broadband THz radiation obtained by non-phase-matched DFG, Cherenkov-type radiation and narrowband THz radiation obtained by quasi-phase-matched DFG in ppLN. Single-cycle broadband as well as tunable narrowband THz radiation has attracted great interest for a wide variety of applications. Beyond these possibilities the use of aperiodically poled crystals opens the opportunity to predefine the shape of the temporal or spectral envelope of the THz radiation or to tune the frequency of the THz radiation generated in sideways direction.

We will focus on the possibility of defining the temporal or spectral shape of the THz radiation. A defined shape of the spectrum can be obtained by predefining a chirp of the fs pulse and using a ppLN crystal [48] or an unmodified fs pulse together with an aperiodically poled LN (AppLN) crystal (a sketch of an AppLN is shown in Fig. 16). For many applications a complex scheme to prechirp the fs pulse according to the needs is not wise. But, the use of aperiodically poled LN allows us to use standard fs pulses.

To understand the idea of using AppLN for this purpose, it is instructive to remember the way in which THz radiation is generated in ppLN. The electric field in the time and frequency domains is determined by the superposition of the waves generated in the particular domains [46]. This can be clearly verified by (33) obtained in Part 1 [1]. The generated spectrum is very sensitive to changes in the domain structure. Even small deviations from the predefined domain structure can be sensitively detected. Lee et al. [51] demonstrated this method. Due to this strong dependency a predefined domain structure can be used to define the THz spectrum. This was proposed and experimentally demonstrated by Lee et al. [52, 53]. A theoretical treatment has been published by Liu et al. [54]. But, these discussions focus on the THz generation in AppLN in the forward direction. This has the disadvantage that for the different frequency components as well as for the partial waves generated in different positions in the sample significantly varying absorption losses occur (see Fig. 9). Therefore, only the remaining part of the radiation contributes to the interference.

The surface scheme which has already been discussed for ppLN (see Sect. 4.2) does not show this problem due to the short path length inside the medium. In addition, AppLN may be of particular interest for easy frequency tuning in the surface emitting scheme. Therefore, we will focus the exemplary discussion on this scheme.

While for bulk LN the length of the sample and for ppLN the length and the periodicity are adequate parameters to characterize the crystal, for AppLN the particular aperiodic structure has to be considered. To allow a discussion we further focus on a special aperiodic structure. In Fig. 17 the photograph and the schematic of the selected AppLN are shown. The sample was poled with a poling period varying from 20 to 254 microns in steps of 13 microns. Each period is repeated four times.

The setup used for the experiments was similar to the one used for common ppLN in the surface emitting scheme discussed in Sect. 4.2. The upper graph of Fig. 18a shows the experimentally obtained electric field of the generated pulse and the lower graph of Fig. 18b indicates the corresponding poling period. For every domain pair, one cycle in the electric field is generated. Four cycles in the electric field correspond to four domain pairs with the same period. As expected from the theoretical discussion [1], every single cycle of the electric field can be predefined by the poling structure. But, this means in accordance with Lee et al. [51–53] that the shape of the electric field (e.g. a linear or quadratic chirp) can be

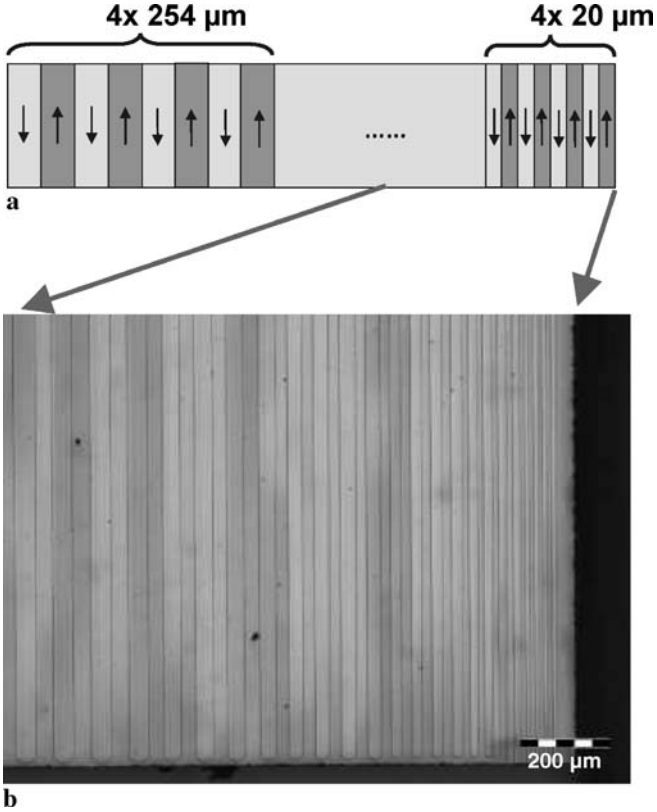

FIGURE 17 Schematic (**a**) and photograph (**b**) of an AppLN crystal for the THz generation in surface emission geometry

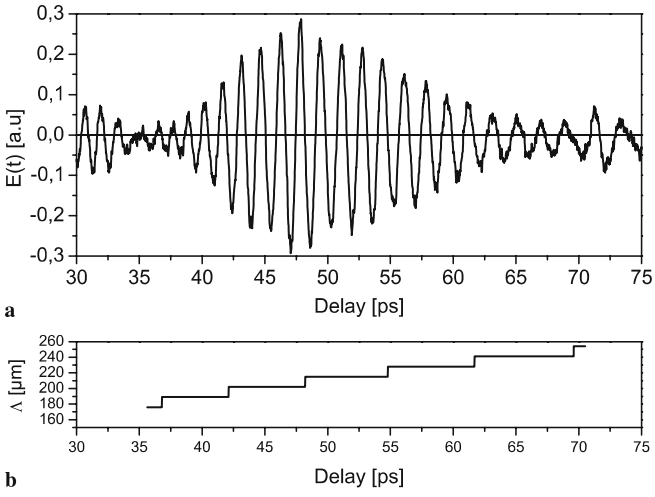

FIGURE 18 Experimentally obtained (**a**) electric field amplitude for an AppLN crystal and (**b**) designed poling period for the AppLN crystal

predefined if the QPM structure of the AppLN is designed accordingly.

A further application of aperiodic structures may be the arrangement of various sets of different poling periods one after another to allow easy frequency tuning in the surface emitting scheme. While the forward scheme has to deal with strong absorption, the surface emitting scheme is limited by the focal length. Only in a short range around the focal point can emission in the sideways direction be obtained (see Sect. 4.2). By defining the position of the focal point of the fs radiation the contributing periods can be selected. This opens a way to overcome one of the remaining limitations of the surface emitting scheme discussed in Sect. 4.2, which is the limit to one or two poling periods near the surface of the crystal. By arranging the various poling periods one after another and adjusting the position of the focus a similar tuning can be obtained in AppLN as in ppLN operated in the forward direction.

6 Tilted periodically poled lithium niobate (TppLN)

THz beams generated in ppLN with standard collinear interaction schemes (see Sect. 4) suffer an essentially reduced output efficiency due to the high absorption. The surface emitting scheme has been offered and demonstrated as an alternative (see Sect. 4.2) to reduce the absorption losses. The main condition which has to be fulfilled was that the optical beam can be focused sharply enough so that the waist diameter is kept smaller than the expected wavelength of the THz radiation. Otherwise, the phase shift between the THz rays generated at different points of the optical beam cross section along the observation direction may exceed π. In this case the different rays would interfere destructively in the detection point.

Because of the damage threshold this condition limited the permitted pump power. Correspondingly lower THz power could be achieved. In the case when longer (e.g. nanosecond) optical pulses should be used, the mentioned limitation could even make the utilization of the surface emitting scheme impossible. One has to note as well that since the smaller waists could be achieved only by sharper focusing, a smaller number of domains could participate in the generation process, and a less-monochromatic THz wave is detected (see Sect. 4.2).

To eliminate the mentioned disadvantages a modified ppLN crystal for surface-emitted THz-wave generation was used. Mainly two poling structures have been discussed and demonstrated for this purpose. A sketch of the poling structure for both schemes is shown in Fig. 19a and c. Besides a chessboard-type poling structure a periodic domain structure oriented under an angle to the crystal edges, a so-called tilted-ppLN (TppLN) or slant-stripe type has been discussed. Since both schemes are very similar in their impact on the THz generation we focus exemplarily on the TppLN scheme. The main idea of the modification is the following: the input and output edges of the rectangular crystal are not cut parallel or perpendicular to the domains of the poled structure but under an angle α as depicted in Fig. 19a. TppLN crystals have been successfully used for surface-emitted THz-wave generation via difference-frequency mixing of optical waves in the nanosecond-duration regime [55] and for the optical rectification of 100-fs pulses at 0.78 μm.

For the experimental demonstration the same setup is used as for the experiments with conventional ppLN in the surface emission scheme in Sect. 4.2. Only the rectangular ppLN crystal has been substituted by a ppLN crystal with tilted periods. The angle α and poling period Λ (the double domain length) were determined from the quasi-phase-matching conditions in both x and y directions [1]:

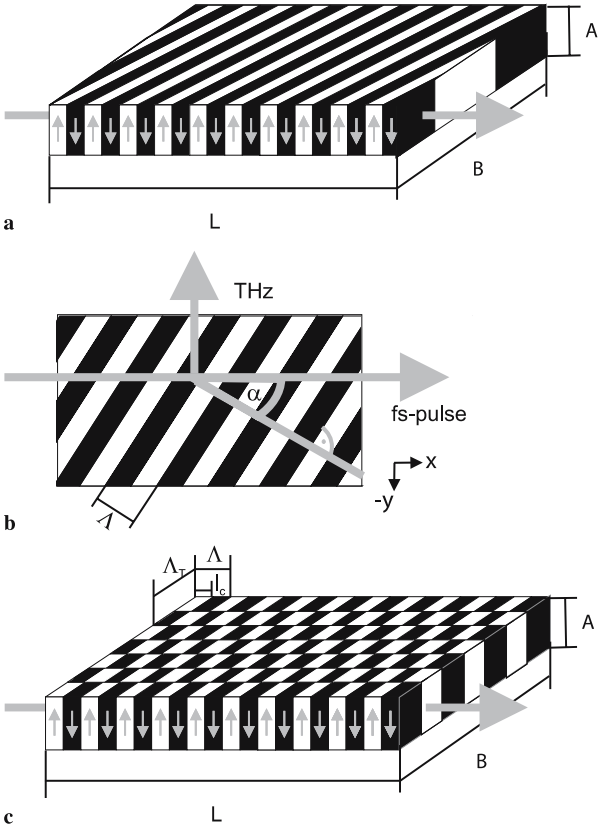

FIGURE 19 The two typically used poling structures to enhance the THz radiation output in the surface emission scheme: (**a**, **b**) slant-stripe type, (**c**) chessboard type. In (**b**) a sketch of the slant-stripe type with the definition of the angle α and the poling period Λ is shown

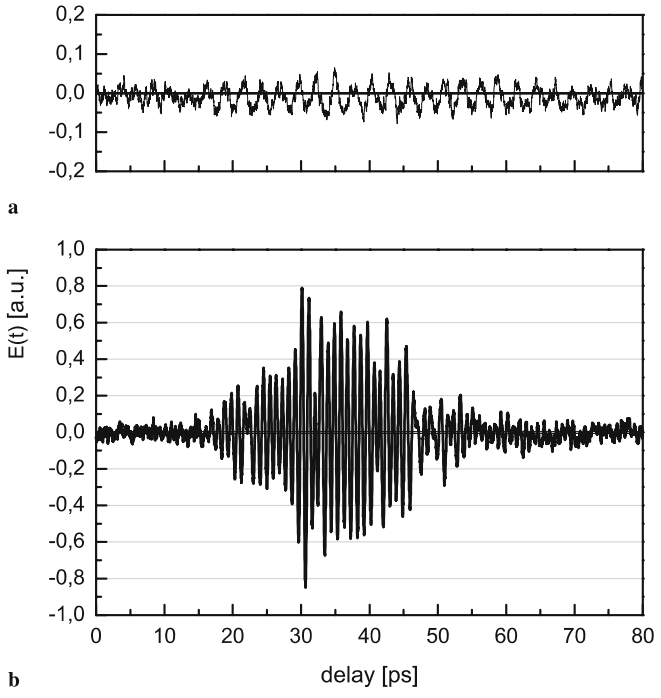

FIGURE 20 Experimentally obtained electric field for a focusing of the fs pulse in the XZ plane with a cylindrical lens ($f = 10$ mm) in (**a**) regular ppLN and (**b**) TppLN

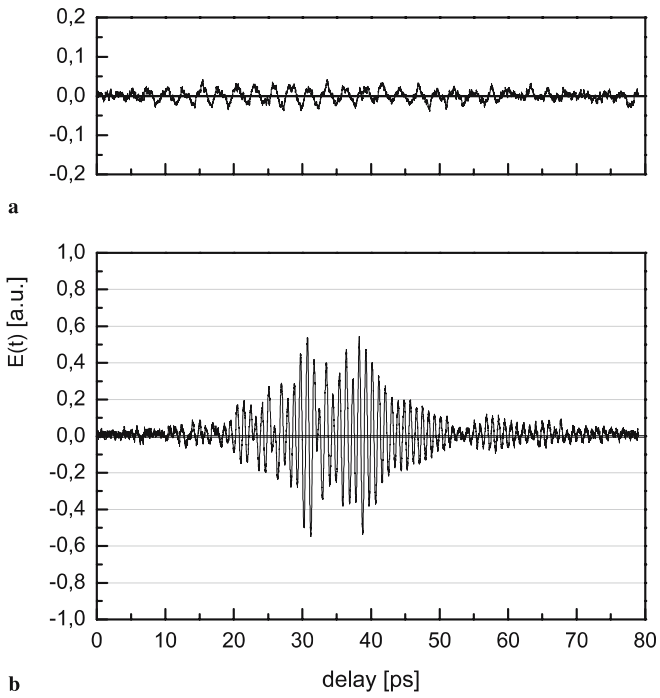

FIGURE 21 Experimentally obtained electric field for a focusing of the fs pulse with a spherical lens ($f = 200$ mm) in (**a**) regular ppLN and (**b**) TppLN

$$\alpha = \arctan\left(\frac{n_{\mathrm{THz}}}{n_{\mathrm{g}}}\right), \tag{9}$$

$$\Lambda = \frac{c}{\nu}\frac{\sin\alpha}{n_{\mathrm{g}}}, \tag{10}$$

where ν is the desired frequency of the THz wave. A sketch of the definition of α and Λ is shown in Fig. 19b.

With $n_{\mathrm{g}} = 2.3$ and $n_{\mathrm{THz}} = 5.17$ for the generation of 1 THz, (9) and (10) result in a poling period of $\Lambda = 56.2\,\mu$m and an angle of $\alpha = 24°$.

To obtain a THz-wave generation around 1 THz in the surface emitting geometry one needs a poling period of 130 μm in the standard orientation (regular ppLN) and a focusing of the pump beam down to a 10-μm to 20-μm waist size. A typical waveform of a THz wave generated by such a regular ppLN crystal is shown in Fig. 15a. A spherical lens ($f =$ 10 mm) was used to generate the waveform shown around 1 THz. When the spherical lens is substituted by a cylindrical lens also of 10-mm focal length, a similar waveform is generated only when the curvature of the lens lay in the XY plane. If, on the contrary, the curvature was in the YZ plane (the beam is not focused along y) then the measured THz radiation is too weak and has a much lower frequency, corresponding to the backward generation as shown in Fig. 20a (see also Fig. 14).

After the regular ppLN crystal was substituted by another with tilted domains under an angle of $\alpha = 23°$ with a period of $\Lambda = 50\,\mu$m (close to the values calculated by (9) and (10)), a stronger emission and a higher frequency (around 1 THz) are generated (Fig. 20b). The parameters of the ppLN crystal are selected so that along the y axis the THz rays generated from neighboring domains interfere constructively. Therefore, the beam size along the y axis has not necessarily to be smaller than the generated wavelength. In that case, the phase difference between the rays generated from different parts of the beam cross section is quasi-compensated by the periodically poled nonlinearity of the crystal in the x direction, hence leading to those rays interfering constructively at the detection point. The demonstrated possibility of using a not very sharply focused pump beam with the tilted ppLN crystal allows in addition for a bigger number of poling domains to be involved in the THz generation process, resulting in a more monochromatic radiation. For demonstration, a spherical lens with a focal length of 200 mm in combination with the same tilted ppLN sample was used. The focal spot size in that case would not be small enough to generate high-frequency THz components in the regular ppLN sample, as demonstrated in Fig. 21a. In the case of tilted ppLN the same focusing geometry generates higher spectral components and a stronger amplitude (Fig. 21b).

7 Conclusion

In conclusion, we have discussed theoretically and experimentally and compared various schemes to generate THz radiation in optical nonlinear crystals using fs NIR radiation. These schemes allow us to produce broadband as well as narrowband but tunable THz radiation.

Following the outline of Part 1 [1], we discussed the generation of THz radiation in bulk LN. While optical rectification is not efficient, due to the missing phase matching, Cherenkov radiation is a suitable scheme to produce broadband radiation. The major task to obtain Cherenkov radiation efficiently is to extract the radiation from the crystal, because the Cherenkov angle is greater than the angle of internal total reflection. Two schemes (wedged crystals and silicon prims) to overcome this problem have been discussed and compared.

To obtain a reasonable amount of Cherenkov radiation it is necessary to sharply focus the NIR beam into the LN crystal, to fulfill momentum conservation. For power scaling it is advantageous to use the tilted pulse front geometry to overcome the problem of optical damage of the crystal.

A very different and versatile approach to obtain phase matching is to use ppLN crystals. This scheme leads to narrowband but tunable radiation. Realizations in the forward as well as in the surface/sideways emitting scheme and possibilities to tune the frequency of the THz radiation have been discussed. The surface emitting scheme has the benefit that the emitted radiation is generated close to the surface. Therefore, only very low absorption losses occur. A promising solution to the necessary sharp focusing to obtain surface-emitted radiation was the use of two-dimensionally structured LN samples.

Aperiodically poled LN has been demonstrated to be a versatile possibility to design the electric field as well as the frequency spectrum of the THz pulse.

Despite the discussion being focused on LN, these results can easily be applied to other nonlinear materials like GaAs, which has a strongly reduced absorption coefficient at THz frequencies.

ACKNOWLEDGEMENTS The authors acknowledge Alexander Quosig for his help in the preparation of samples for the experiments.

REFERENCES

1 J. A. L'huillier, G. Torosyan, M. Theuer, Y. Avetisyan, R. Beigang, Appl. Phys. B (2006), DOI: 10.1007/s00340-006-2490-9
2 K. Kawase, M. Sato, T. Taniuchi, H. Ito, Appl. Phys. Lett. **68**, 2483 (1996)
3 A. Stepanov, J. Hebling, J. Kuhl, Appl. Phys. B **81**, 23 (2005)
4 Y. Avetisyan, Y. Sasaki, H. Ito, Appl. Phys. B **73**, 511 (2001)
5 J. Hebling, A. Stepanov, G. Almaasi, B. Bartal, J. Kuhl, Appl. Phys. B **78**, 593 (2004)
6 M. Theuer, G. Torosyan, C. Rau, R. Beigang, K. Maki, C. Otani, K. Kawase, Appl. Phys. Lett. **88**, 071 122 (2006)
7 C. Weiss, G. Torosyan, J. Meyn, R. Wallenstein, R. Beigang, Y. Avetisyan, Opt. Express **8**, 497 (2001)
8 A. Stepanov, J. Kuhl, I. Kozma, E. Riedle, G. Almasi, J. Hebling, Opt. Express **13**, 5762 (2005)
9 P. Jepsen, C. Winnewisser, M. Schall, V. Schyja, S. Keiding, H. Helm, Phys. Rev. E **53**, R3052 (1996)
10 A. Rice, Y. Jin, X.F. Ma, X.C. Zhang, D. Bliss, J. Larkin, M. Alexander, Appl. Phys. Lett. **64**, 1324 (1994)
11 D. Zheng, L.A. Gordon, Y.S. Wu, R.S. Feigelson, M.M. Fejer, R.L. Byer, K.L. Vodopyanov, Opt. Lett. **23**, 1010 (1998)
12 W. Shi, Y. Ding, N. Fernelius, K. Vodopyanov, Opt. Lett. **27**, 1454 (2002)
13 W. Shi, Y. Ding, Appl. Phys. Lett. **84**, 1635 (2004)
14 W. Shi, Y.J. Ding, P.G. Schunemann, Opt. Commun. **233**, 183 (2004)
15 K. Kawase, M. Mizuno, S. Sohma, H. Takahashi, T. Taniuchi, Y. Urata, S. Wada, H. Tashiro, H. Ito, Opt. Lett. **24**, 1065 (1999)
16 K. Kawase, T. Hatanaka, H. Takahashi, K. Nakamura, T. Taniuchi, H. Ito, Opt. Lett. **25**, 1714 (2000)
17 A. Nahata, D.H. Auston, C.J. Wu, J.T. Yardley, Appl. Phys. Lett. **67**, 1358 (1995)
18 A. Sinyukov, M. Leahy, L. Hayden, M. Haller, J. Luo, A. Jen, L. Dalton, Appl. Phys. Lett. **85**, 5827 (2004)
19 D.A. Roberts, IEEE J. Quantum Electron. **QE-28**, 2057 (1992)
20 A. Harada, Y. Nihei, Appl. Phys. Lett. **69**, 2629 (1996)
21 L.E. Myers, R.C. Eckardt, M.M. Fejer, R.L. Byer, Opt. Lett. **21**, 591 (1996)
22 G.D. Miller, Periodically poled lithium niobate: modelling, fabrication, and nonlinear-optical performance, Ph.D. thesis, Stanford University (1998)
23 M. Yamada, N. Nada, M. Saitoh, K. Watanabe, Appl. Phys. Lett. **62**, 435 (1993)
24 L. Palfalvi, J. Hebling, J. Kuhl, A. Peter, K. Polgar, J. Appl. Phys. **97**, 123 505 (2005)
25 M. Schall, H. Helm, S. Keiding, Int. J. Infrared Milli. **20**, 595 (1999)
26 D.A. Bosomword, Appl. Phys. Lett. **9**, 330 (1966)
27 H.J. Bakker, S. Hunsche, H. Kurz, Phys. Rev. B **50**, 914 (1994)
28 J. Shikata, M. Sato, T. Taniuchi, H. Ito, K. Kawase, Opt. Lett. **24**, 202 (1999)
29 M. Bass, P.A. Franken, J.F. Ward, G. Weinreich, Phys. Rev. Lett. **9**, 446 (1962)
30 A. Nahata, A.S. Weling, T.F. Heinz, Appl. Phys. Lett. **69**, 2321 (1996)
31 L. Xu, X.C. Zhang, D.H. Auston, Appl. Phys. Lett. **61**, 1784 (1992)
32 T.J. Carrig, G. Rodriguez, T.S. Clement, A.J. Taylor, K.R. Stewart, Appl. Phys. Lett. **66**, 121 (1995)
33 G.A. Askaryan, Sov. Phys. JETP **15**, 943 (1962)
34 D.H. Auston, K.P. Cheung, J.A. Valdmanis, D.A. Kleinman, Phys. Rev. Lett. **53**, 1555 (1984)
35 D.A. Bagdasaryan, A.H. Makaryan, P. Pogosyan, JETP Lett. **37**, 594 (1983)
36 B.B. Hu, X.C. Zhang, D.H. Auston, Appl. Phys. Lett. **56**, 506 (1990)
37 K. Kawase, M. Sato, K. Nakamura, T. Taniuchi, H. Ito, Appl. Phys. Lett. **71**, 753 (1997)
38 D. Grischkowsky, S. Keiding, M. van Exter, C. Fattinger, J. Opt. Soc. Am. B **7**, 2006 (1990)
39 G.D. Boyd, D.A. Kleinmann, J. Appl. Phys. **39**, 3597 (1968)
40 M.M. Fejer, G.A. Magel, D.H. Jundt, R.L. Byer, IEEE J. Quantum Electron. **QE-28**, 2631 (1992)
41 J. Meyn, M. Klein, D. Woll, R. Wallenstein, D. Rytz, Opt. Lett. **24**, 1154 (1999)
42 R. Huber, A. Brodschelm, F. Tauser, A. Leitenstorfer, Appl. Phys. Lett. **76**, 3191 (2000)
43 J. Hebling, G. Almasi, I. Kozma, J. Kuhl, Opt. Express **10**, 1161 (2002)
44 Y. Lee, T. Meade, M. DeCamp, T. Norris, A. Galvanauskas, Appl. Phys. Lett. **77**, 1244 (2000)
45 Y. Lee, T. Meade, V. Perlin, H. Winful, T. Norris, A. Galvanauskas, Appl. Phys. Lett. **76**, 2505 (2000)
46 Y. Lee, T. Meade, T. Norris, A. Galvanauskas, Appl. Phys. Lett. **78**, 3583 (2001)
47 C. Weiss, G. Torosyan, Y. Avetisyan, R. Beigang, Opt. Lett. **26**, 563 (2001)
48 J. Ahn, A. Efimov, R. Averitt, A. Taylor, Opt. Express **11**, 2486 (2003)
49 U. Strossner, J. Meyn, R. Wallenstein, P. Urenski, A. Arie, G. Rosenman, J. Mlynek, S. Schiller, A. Peters, J. Opt. Soc. Am. B **19**, 1419 (2002)
50 Y.H. Avetisyan, K.N. Kocharian, A new method of terahertz difference frequency generation using periodically poled waveguide, in *CLEO 1999 Tech. Dig.*, 1999, pp. 380–381
51 Y.S. Lee, T. Meade, M.L. Naudeau, T.B. Norris, A. Galvanauskas, Appl. Phys. Lett. **77**, 2488 (2000)
52 Y. Lee, T. Norris, J. Opt. Soc. Am. B **19**, 2791 (2002)
53 Y. Lee, N. Amer, W. Hurlbut, Appl. Phys. Lett. **82**, 170 (2003)
54 X. Liu, J. Wu, W. Duan, B. Gu, J. Appl. Phys. **97**, 114 108 (2005)
55 Y. Sasaki, Y. Avetisyan, K. Kawase, H. Ito, Appl. Phys. Lett. **81**, 3323 (2002)